第 34 卷第 3 期
2018 年 3 月

无 机 化 学 学 报
CHINESE JOURNAL OF INORGANIC CHEMISTRY

Vol.34 No.3
597-604

三维树枝状银薄膜的可控生长及其在表面增强拉曼光谱中的应用

张慧娟 张东杰 张丛筠* 刘亚青*
(中北大学功能纳米复合材料山西省重点实验室,太原 030051)

摘要:通过电流置换反应制备了树枝状银纳米薄膜。在反应过程中通过控制反应时间和硝酸银的浓度,得到了不同形貌、分布和密度的树枝状银薄膜,从而得到了具有不同 SERS 性能的树枝状银纳米薄膜。选取了具有最佳 SERS 性能的树枝状银纳米薄膜对罗丹明 6G 进行了微量检测、再现性检测和稳定性检测,其检测限可达到 1×10^{-11} mol·L^{-1},具有优良的再现性和良好的稳定性。

关键词:银树枝状膜;表面增强拉曼散射;电流置换反应
中图分类号:O614.122 **文献标识码**:A **文章编号**:1001-4861(2018)03-0597-08
DOI:10.11862/CJIC.2018.085

3D Silver Dendritic Thin Film: Controllable Growth and Application in Surface Enhanced Raman Spectroscopy

ZHANG Hui-Juan ZHANG Dong-Jie ZHANG Cong-Yun* LIU Ya-Qing*
(*Shanxi Province Key Laboratory of Functional Nanocomposites, School of Materials Science and Engineering, North University of China, Taiyuan* 030051, *China*)

Abstract: A novel surface enhanced Raman spectroscopy (SERS) substrate was fabricated via a simple galvanic displacement reaction, where large scale of silver dendritic were uniformly and symmetrically formed on anodic aluminum oxide (AAO) membrane. The morphology, distribution and density of these silver dendritic films could be tuned easily just by controlling the reaction time as well as the concentration of $AgNO_3$. Such active SERS substrate exhibits extremely high sensitivity, excellent reproducibility and good stability. Raman signal sensitivity for rhodamine 6G (R6G) was tested as low as 1×10^{-11} mol·L^{-1}. Additionally, the as-synthesized robust substrate displays good stability under an ambient condition for several months. This 3D eco-friendly AAO membrane based substrate provides not only high density of SERS hot spots, but also a very large area for capturing target analytes. It has potential applications for the detection of trace organic contaminants in the environment.

Keywords: silver dendritic films; SERS; galvanic displacement reaction

0 Introduction

Surface enhanced Raman spectroscopy (SERS), a highly sensitive and convenient analytical method, which could provide rich fingerprint structure information. It has been intensely researched for many years in the fields of medicine, analytical chemistry, surface science, and so on[1-3]. To date, a number of nanostructures (Au, Ag) have been fabricated as SERS substrates for acquiring remarkable SERS signal enhancement[4], especially the structure of gold[5], silver[6] and copper[7]. Among them, the performance of silver is best, due to their unique electrical and tunable localized surface plasmon resonance (LSPR) properties. So silver nanostructures with various morphologies are studied, such as roughened plasmonic

收稿日期:2017-11-28。收修改稿日期:2018-01-10。
山西省青年科学家自然科学基金(No.2015021078)和中国山西省科学技术项目国际合作(No.201603D421030)资助项目。
*通信联系人。E-mail:z.congyun@nuc.edu.c;lyq@nuc.edu.cn

nanoarrays[8-9], nanorods[10], core-shell nanostructures[11-13], Ag nanowires[14], dendrites[15-16], Ag nanosheets[17], "flower like" nanoparticles[18-19], Ag nanocubes[20] and other complex hierarchical structures[21].

Among all these substrates, silver dendrites have received considerable attention, because of their multilevel generations of branches with self-similarity and periodic arrangement which can increase the specific surface area and generate many spots with huge coupling effect (so-called as "hot spots")[22] . So a lot of promising dendritic Ag structures acted as SERS substrates have been developed and used for various applications. For instance, Wang et al.[23] detected 2-MBT using a silver dendrites formed by a self-assembled fabrication approach with a detection limit of 10^{-10} mol·L^{-1}. Hu et al.[24] prepared an ultrastable SERS substrates based on Ag dendritic nanostructures coated with silica nanofilm, which possessed significant potential for rapid, sensitive and quantitative detection of organic molecules. Zuo et al.[25] synthesized ordered Ag nanodendrite cluster arrays to detect rhodamine 6G with the concentration as low as 10 pmol·L^{-1}. Meanwhile, they examined their SERS-sensitivity to thiram with a limitation to 10^{-5} mol·L^{-1}. However, it is still a challenge to prepare a SERS substrate with high sensitivity, stability, and reproducibility for trace detection of target molecules at the same time.

Herein, silver dendritic films with large covering densities have been synthesized based on anodic aluminum oxide (AAO) membrane by a simple galvanic displacement reaction. This method was conducted at room temperature preparation without using any surfactants. The morphology, distribution and density of these silver dendritic films could be tuned easily just by controlling the reaction time as well as the concentrations of $AgNO_3$. Using these silver dendritic films as SERS substrates, Raman signal of rhodamine 6G (R6G) with different concentrations can be obtained due to numerous hot spots on the substrates. The limits of detection (LOD) for R6G could be reached 10^{-11} mol·L^{-1}. Moreover, a good reproducibility and stability can be also obtained for this SERS substrate, indicating a promising application for SERS detection.

1 Experiment

1.1 Materials

Silver nitrate ($AgNO_3$, ACS, 99.9%) was purchased from Alfa Aesar. AAO membrane was supplied by Whatman International Corp. All chemical reagents were analytical grade and used without any purification. All glass containers were rinsed with aqua regia (V_{HCl}:V_{HNO_3}=3:1) before used, and then rinsed with ultrapure water (the resistivity of 18.2 MΩ·cm^{-1}, Millipore) several times.

1.2 Synthesis of silver dendritic thin film

For the preparation of silver dendritic thin film, the bottom side of AAO membrane was firstly sputter-deposited with thin copper film of 500 nm through thermal evaporator. Subsequently, silicon wafer, AAO (sputtered with Cu membrane), O ring, and a teflon cell were assembled into the above reaction device which was sealed to avoid the overflowing of reaction solutions by clamps (Fig.1a). Finally, $AgNO_3$ (5 mL, 0.1 mol·L^{-1}) was added into the reaction device slowly, and then AAO was taken out 10 minutes later. It was obvious that the upper side of the AAO was changed into silvery white, indicating the occurrence of silver dendritic thin film. The samples were washed with ultrapure water for several times, and then dried at room temperature for 24 h. In order to obtain the optimal morphology and distribution of dendritic silver films, controlled experiments were conducted by changing the reaction time and the concentrations of $AgNO_3$, respectively.

1.3 Characterization

The distribution, size and morphology of the synthesized silver dendritic thin film were characterized by a scanning electron microscope (SEM, Tescan MIRA 3LMH, U=15 kV, I=10 mA), a transmission electron microscope (TEM, JEOL 2100F, U=120 kV) and a high resolution TEM (HRTEM, JEOL 2100F, U=200 kV). X-ray diffraction (XRD) data of the as-prepared samples were recorded from a Bruker D8 focus diffractometer with Cu $K\alpha$ source (λ=0.154 16 nm). The scanning angle range (2θ) is from 30° to 80°

with scanning speed of 1°·min^{-1}. The corresponding working voltage and current were 40 kV and 40 mA, respectively.

1.4 SERS measurements

For SERS measurement, the samples were prepared by drop-casting 0.1 mL of 10^{-6} mol·L^{-1} rhodamine 6G (R6G) solutions onto the silver dendrite-integrated AAO membrane and dried in atmosphere. The samples were rinsed with ultrapure water for several times and dried in dark at ambient condition again. Bare AAO membrane with 500 nm Cu film was also immersed in 10^{-2} mol·L^{-1} R6G solution for comparison. The Raman scattering measurements were conducted on a confocal microprobe Raman system (Renishaw invia) through a 50 L×objective, and the excitation wavelength was 785 nm with a power of 9 mW. The total acquisition time was 10 s for each spectrum.

2 Results and discussion

2.1 Structure and characterization

The size and morphology of AAO membrane used in the experiment could be seen in Fig.S1A (Supporting Information). The diameter of the inner pores was about 200 nm, and the thickness was ~60 μm. Fig.S1B shows the bottom side of the AAO membrane, sputtered with 500 nm Cu films. In the experiment, the aqueous silver nitrate contacted with the Cu layer through the inner pores of AAO membrane (inset in Fig.S1A), and then silver dendritic thin film was obtained by growing through the inner pores.

When the concentration of $AgNO_3$ was 0.1 mol·L^{-1} with reaction time for 10 min, SEM images of the products reveal the 3D networked dendritic silver nanostructures on the upside of AAO membrane (Fig. 1 (a)). It can be seen that the large scale of dendritic

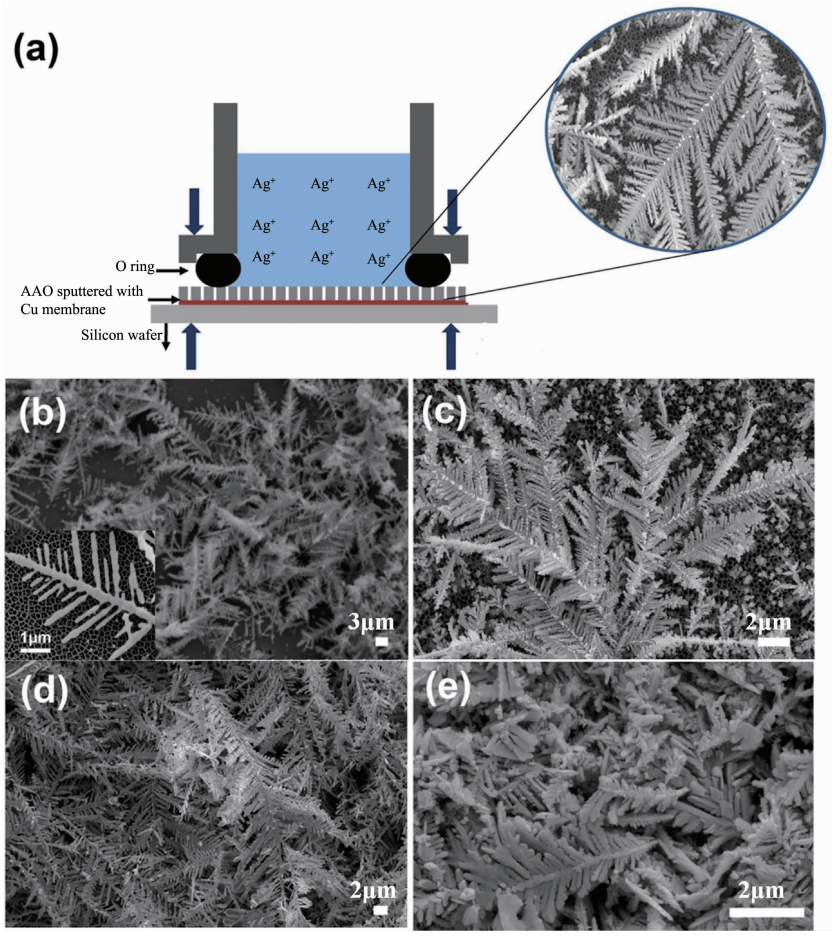

Fig.1 (a) Illustration of the growth device of silver dendritic thin film; (b~e) SEM images of the silver dendritic thin film with different reaction times of (b) 1 min (c) 5 min (d) 10 min and (e) 1 h

samples are formed into a thin film above the AAO membrane with a fairly high rate of coverage. The length of the main trunk is about 20 μm while the length of the average side branches is around 5 μm. SEM image in Fig.1(b) is a main branch of the dendritic structure in Fig.1(a), which also confirms that these silver dendrites are well defined, uniform and ordered with pronounced trunk and smaller branches on both sides of the trunk. Moreover, these sub-branches align with an angle of ~60° to the main branches, showing a symmetrical structure.

The morphology and structure were further confirmed by TEM, selected area electron diffraction (SAED) and XRD (Fig.2(a~f)). The Dark field TEM images and SAED illustrate the crystalline nature of the silver dendrites (Fig.2(c~d)). The SAED patterns was recorded from a tip of a small branch, showing regular hexagonal diffraction spot array. The crystal orientation and growth direction of the silver dendrite can be obtained, indicating that the whole dendrite is a single crystal represented by facets. Further insight into the Ag dendrites has been obtained by HRTEM images (Fig.2(e)), which consists of the tip area of the main branch. The results show that the distance between the lattice planes is 0.204 nm, which is in agreement with *d* spacing of face centered cubic (*fcc*) structures (PDF No.87-0597). Fig.2(f) illustrates the XRD pattern of silver dendritic films adsorbed on the AAO membrane, also confirming the crystalline nature of the products. The peaks at 38.3°, 44.3°, 64.4° and 77.5° are obtained, corresponding to the (111), (200), (220) and (311) crystal plane respectively, which confirms the presence of face centered cubic pattern (PDF No.87-0597) [26]. The peak at 38.3° corresponding to (111) plane is found to be of high intensity compared to other planes, indicating that the silver dendrites preferentially grows along the (111) plane.

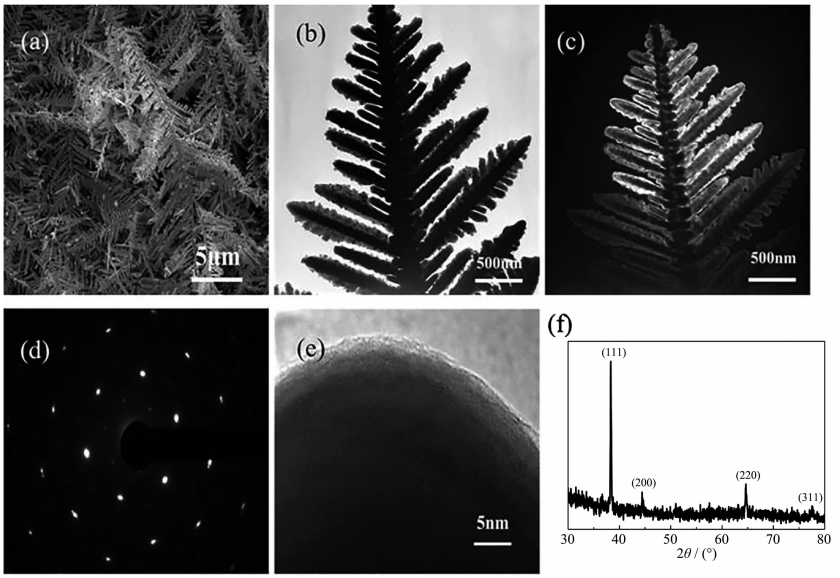

Fig.2 Silver dendritic thin film prepared at 0.1 mol·L^{-1} of silver nitrate (aqueous) for 10 min; (a) SEM images; (b) TEM images; (c) Dark field TEM images; (d) Selected area electron diffraction (SAED) pattern; (e) HRTEM image; (f) X-ray diffraction (XRD) pattern

2.2 Time evolution study

It is known that a strong anisotropic growth contributes to the evolution of silver nanostructure into a thermodynamic stable dendritic structure[27]. However, it is difficult to predict the reaction time for the formation of dendritic structure. In order to study the influence of the reaction time, the growth of dendritic silver films was carried out at reaction times ranging from 1 min to 3 h, with a constant $AgNO_3$ concentration of 0.1 mol·L^{-1}. As the reaction time ranging from 1 min to 3 h, the rate of coverage on the AAO membrane becomes higher (Fig.S2), while the

coverage is still very high especially when the reaction time is 1 min. As shown in Fig.3, when the reaction time is very short (1 min), the growth process is dominated by a nonequilibrium condition[28], so silver dendritic structures are always formed with broken branches, and the thickness of these branches is small. Moreover, some distinct silver nanoparticles can be found around the defective dendritic products, indicating the nanoparticle aggregation based growth. By 5 min, the crystals have developed into well-defined dendritic structures. During this period, the tips of the main trunk start to divided into some smaller branches (Fig.3 (c)). High-magnification SEM image in Fig.3(d) is a smaller trunk in Fig.3(c), which indicates the appearance of secondary branches. As the growth process extend to 10 min, the morphology of the dendrites gradually develop to unbroken structure, and the branches on trunks arrang more symmetrically. After 1 and 3 h, the length of trunks increase and more secondary branches appeared, which indicates the transform process from quasi-equilibrium to equilibrium conditions. It is noteworthy that tertiary branches came into being on secondary branches (Fig.3(e~h)). Many silver nanoparticles adsorb on the tertiary branches, which can be seen in Fig.3 (f). Moreover, the tertiary branches and silver nanoparticles on them start to fuse together, and the surface of the dendritic structures became smooth, which is thermodynamically stable. The relationship between morphological evolution and SERS signal were investigated, in which the AAO-based dendrites obtained at 1 h reaction time show the best SERS sensitivity (Fig.S3).

The growth process above could be explained by a diffusion limited aggregate mechanism[29]. It is illustrated that the formation of the dendritic structure is based on the asymmetric growth of silver nanoparticles. At the beginning stage, the growth rate of dendrites is controlled by the rate of Ag^+ diffusion to the interface. After the galvanic displacement reaction, Ag^+ converts into Ag nanoparticles, and then silver nanoparticles start to grow along the (111) direction, due to the growth process is more prone to along the (111) direction to form a trunk. As the growth process continues, more and more silver nanoparticles are formed, and these additional silver nanoparticles move randomly to a low energy position and attach to the silver trunk. Moreover, these attach silver nanoparticles grow still along the (111) direction, further resulting in the secondary and tertiary branches. Lastly, all the prepared trunks, branches grow and interconnect to each other finally, and a whole silver dendritic structure is formed when the growth process take place repeatedly.

2.3 Effects of $AgNO_3$ concentrations

The morphology of a crystal structure is affected by the relationship between the growth condition and the equilibrium state, such as the driving force for

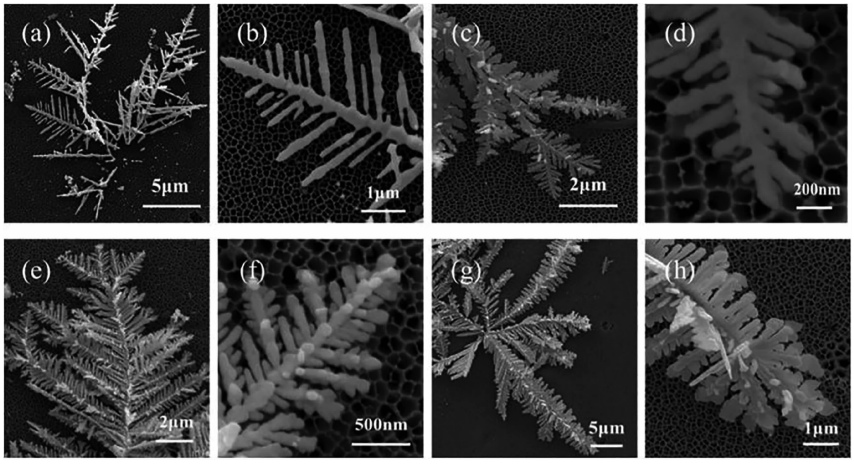

(a, b) 1 min; (c, d) 5 min; (e, f) 1 h; (g, h) 3 h; Concentration of silver nitrate is 0.1 mol·L^{-1}

Fig.3　SEM images of the silver dendritic thin film with different reaction times

crystallization. For the syntheses of the silver dendritic films in this case, the driving force depends on the degree of supersaturation. Higher concentration of Ag^+ can enhance the reaction rate greatly, leading to huge changes in the morphology and distribution of silver dendritic films. Therefore, a series of $AgNO_3$ concentrations were selected to investigate their effects to the formation of silver dendrites. Fig.4 illustrates the growth process of silver dendrites at various concentrations (0.01, 0.05, 0.1, 0.5 mol·L^{-1}) for a reaction time of 10 min, and a drastic change is observed.

When the concentration of $AgNO_3$ was 0.01 mol·L^{-1}, only many dispersive silver nanoparticles were obtained without any appearance of dendritic nanostructures, indicating that low concentration can led to incomplete morphologies. As the concentration added to 0.05 mol·L^{-1}, a broken dendritic silver nanostructure appeared with some imperfect branches, indicating that a higher concentration can promotes the transition from incomplete structure to dendritic growth. By 0.1 mol·L^{-1}, a whole dendritic sample can be formed with symmetrical branches. However, higher concentration will not be helpful for the controllable formation of silver dendritic structures due to too fast reaction (Fig.4(d)). Although the morphology of the silver structure is still dendrite, however, the thickness of the trunk and branches are very large with many huge silver nanoparticles on the surface. This experiment indicates that a silver dendritic structure with well-defined morphology can be obtained just by controlling the concentration of silver nitrite in the solution.

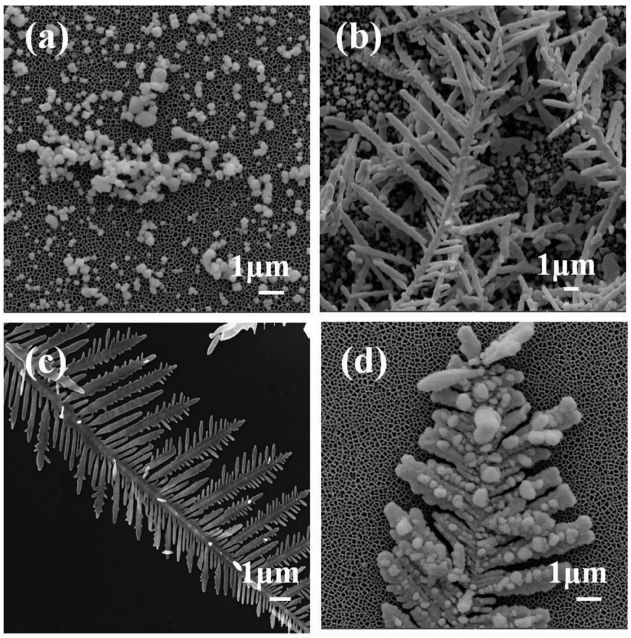

(a) 0.01, (b) 0.05, (c) 0.1 and (d) 0.5 mol·L^{-1}; Reaction time for each concentration is 10 min

Fig.4 SEM images of the silver dendritic thin film with different concentrations of $AgNO_3$

2.4 SERS activity, stability and reproducibility

In order to study the SERS properties of the dendritic silver thin films adsorbed on AAO membranes, R6G with different concentration were utilized as probe molecules. The Raman spectra (Fig.5a) show the major vibrational peaks of R6G at 613, 776, 1 185, 1 312, 1 364, 1 511, 1 576, and 1 651 cm^{-1}, which are attributed to the plane bending of C-C-C ring, out-of-plane bending of the hydrogen atoms within the xanthene skeleton, C-C stretching vibrations, and the aromatic stretching vibrations[30], respectively. It is notable that the ultrasensitive molecular sensing for R6G is as low as 10^{-11} mol·L^{-1}. The inset shown in Fig.5(a) shows the intensities of representative band at 1 364 cm^{-1} against the logarithmic concentration of R6G. It is noteworthy that the R6G molecules present a good signal-to-noise ratio, even for the concentrations down to 10^{-11} mol·L^{-1}, and the distinctive and

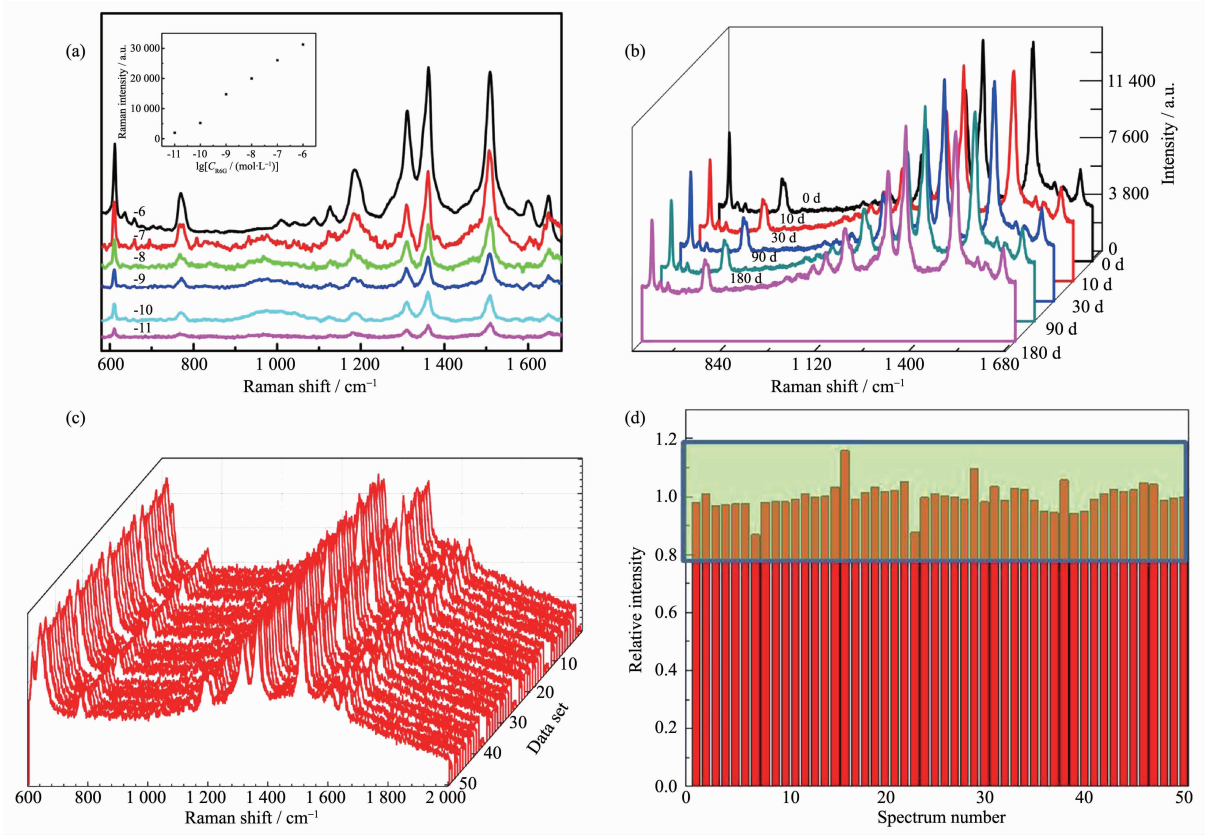

Fig.5　(a) SERS spectra of R6G with different concentrations on the silver dendritic thin film (from 10^{-6} to 10^{-11} mol·L^{-1}), (inset Plot of signal intensity of R6G at 1 364 cm^{-1} versus logarithmic R6G concentration); (b) SERS spectra of R6G adsorbed on the silver dendritic thin film with different exposure time (from 0 to 180 days); (c) SERS spectra of R6G randomly recorded at 50 positions from prepared SERS substrates, the inset shows the SERS intensity maps at the band of 1 364 cm^{-1}; (d) Intensity distribution of the 1 364 cm^{-1} peak of the 50 spectra

characteristic peaks of R6G can be still discernable at 10^{-11} mol·L^{-1}, indicating a great sensitivity in molecule detection. The stability of the SERS substrate is another important factor for the practical application. Therefore, to study the shelf-life of silver substrates, the as-prepared silver dendritic films exposed under ambient conditions for different days (0~180 days) was tested (Fig.5b). The results show no distinct changes in either the intensity or the position of the R6G spectral peaks, indicating good stability of the silver dendritic SERS substrate.

In order to evaluate the reproducibility of the silver dendritic SERS substrates, Raman spectra of R6G molecules with a concentration of 10^{-6} mol·L^{-1} were collected randomly from different positions. The result in Fig.5(c) shows a satisfactory consistency of the SERS performance. The relative intensity distribution at typical peaks of 1 364 cm^{-1} of the SERS substrate shows the relative intensity deviation is less than 20% in total, demonstrating a good reproducibility of SERS signals Fig.5(d).

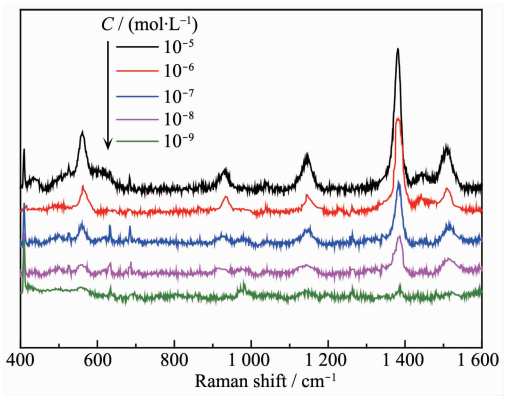

Fig.6　SERS spectra of thiram with different concentrations on the silver dendritic thin film (from 10^{-5} to 10^{-9} mol·L^{-1})

To evaluate the potential application in real-world samples, the as-prepared SERS substrates were tested using thiram as probe molecules. The detected minimum concentration of thiram is as low as 1×10^{-9} mol·L^{-1}, indicating a promising potential for real-world monitoring of trace organic pollutants.

3 Conclusions

AAO membrane modified with Ag dendrites were successfully fabricated and acted as an effective 3D SERS substrates. The morphologies of Ag dendritic structures can be facilely controlled by changing the reaction time and the concentrations of $AgNO_3$. These results also indicate that the significance of gap separation between neighboring branches or sub-branches and the sub-branches couplings in the overall electric field enhancements for the AAO based SERS substrate. The as-synthesized 3D substrate with special structures could generate abundant of hot spots and provide large surface to loading analyte molecules. This flexible, robust and eco-friendly SERS substrate presents extremely high sensitivity, high reproducibility and stability, which can potentially be used for trace detection of organic pollutants in environment.

Acknowledgments: This work was supported by the Natural Science Foundation for Young Scientists of Shanxi Province of China (Grant No.2015021078) and International Coopera-tion of Science and Technology Project in Shanxi Province of China (Grant No.201603D421030).

Supporting information is available at http://www.wjhxxb.cn

References:

[1] Schlucker S. *Angew. Chem. Int. Ed.*, **2014**,**53**:4756-4795

[2] Cialla D, Marz A, Bohme R, et al. *Anal. Bioanal. Chem.*, **2012**,**403**:27-54

[3] Lei Y, Yang S K, Wu M H, et al. *Chem. Soc. Rev.*, **2011**,**40**:1247-1258

[4] ZHOU Xin(周鑫), YAO Ai-Hua(姚爱华), ZHOU Tian(周田), et al. *Chem. J. Chinese Universities*(高等学校化学学报), **2014**,**30**(3):543-549

[5] XU Ling(徐玲), YAO Ai-Hua(姚爱华), XU Yan(胥岩), et al. *Chinese J. Inorg. Chem.*(无机化学学报), **2016**,**32**(12):2183-2190

[6] HUANG Qing-Li(黄庆利), ZHU Xia-Shi(朱霞石). *Chinese J. Inorg. Chem.*(无机化学学报), **2014**,**30**(2):442-450

[7] MAN Shi-Qing(满石清), XIAO Gui-Na(肖桂娜). *Chinese J. Inorg. Chem.*(无机化学学报), **2009**,**25**(7):1279-1283

[8] Yang S K, Slotcavage D, Mai J D, et al. *J. Mater. Chem. C*, **2014**,**2**:8350-8356

[9] Cheng Z Q, Nan F, Yang D J, et al. *Nanoscale*, **2015**,**7**:1463-1470

[10]Huang Z L, Meng G W, Huang Q, et al. *J. Raman Spectrosc.*, **2013**,**44**:240-246

[11]Rong Z, Xiao R, Wang C W, et al. *Langmuir*, **2015**,**29**:8129-8137

[12]Guo P Z, Sikdar D, Huang X Q, et al. *Nanoscale*, **2015**,**7**:2862-2868

[13]LI Jian-Feng(李剑锋), HU Jia-Wen(胡家文), REN Bin(任斌), et al. *Acta Phys.-Chim. Sin.*(物理化学学报), **2005**,**21**(8):825-828

[14]Tao A, Kim F, Hess C, et al. *Nano Lett.*, **2003**,**3**:1229-1233

[15]Chan Y F, Zhang C X, Wu Z L, et al. *Appl. Phys. Lett.*, **2013**,**102**:183118

[16]Laurier K G M, Poets M, Vermoortele F, et al. *Chem. Commun.*, **2012**,**48**:1559-1561

[17]Zhu C H, Meng G W, Huang Q, et al. *Chem. Commun.*, **2011**,**47**:2709-2711

[18]Liang H Y, Li Z P, Wang W Z, et al. *Adv. Mater.*, **2009**,**21**:1-5

[19]Xie J P, Zhang Q B, Lee J Y, et al. *ACS Nano*, **2008**,**2**:2473-2480

[20]McLellan J M, Li Z Y, Siekkinen A R, et al. *Nano Lett.*, **2007**,**7**:1013-1017

[21]Li X D, Li M C, Cui P, et al. *CrystEngComm*, **2014**,**16**:3834-3838

[22]Xie S P, Zhang X C, Xiao D, et al. *J. Phys. Chem. C*, **2011**,**115**:9943-9951

[23]Wang X, Liu X H, Wang X. *J. Mol. Struct.*, **2011**,**997**:64-69

[24]Hu Y S, Jeon J, Seok T J, et al. *ACS Nano*, **2010**,**4**:5721-5730

[25]Zuo J, Meng G W, Zhu C H, et al. *RSC Adv.*, **2016**,**6**:26490-26494

[26]Fang J X, You H J, Kong P, et al. *Cryst. Growth Des.*, **2007**,**7**:864-867

[27]Alam M M, Ji W, Luitel H N, et al. *RSC Adv.*, **2014**,**4**:52686-52689

[28]Jiang Z Y, Lin Y, Xie Z X. *Mater. Chem. Phys.*, **2012**,**134**:762-767

[29]Zhu S Q, Zhang T, Guo X L, et al. *Nanoscale Res. Lett.*, **2014**,**9**:114

[30]Xu H Y, Shao M W, Chen T, et al. *J. Raman Spectrosc.*, **2012**,**43**:396-404